

# A cell-based smoothed finite element method for free vibration analysis of a rotating plate

\*C.F. Du<sup>1</sup>, †D.G. Zhang<sup>1</sup>, G.R. Liu<sup>2</sup>

<sup>1</sup> School of Sciences, Nanjing University of Science and Technology, Nanjing 210094, China

<sup>2</sup> Department of Aerospace Engineering and Engineering Mechanics  
University of Cincinnati, Cincinnati, OH 45221, USA

\*Presenting author: [duchaofan1987@163.com](mailto:duchaofan1987@163.com)

†Corresponding author: [zhangdg419@mail.njust.edu.cn](mailto:zhangdg419@mail.njust.edu.cn)

## Abstract

A cell-based smoothed finite element method (CS-FEM) is formulated for non-linear free vibration analysis of a plate attached to a rigid rotating hub. The first-order shear deformation theory which is known as Mindlin plate theory is used to model the plate. In the process of formulating the system stiffness matrix, the discrete shear gap (DSG) method is used to construct the strains to overcome the shear locking issue. The effectiveness of the CS-FEM is first demonstrated in some static cases and then extended for free vibration analysis of a rotating plate considering the non-linear effects arising from the coupling of vibration of the flexible structure with the undergoing large rotational motions. The nonlinear coupling dynamic equations of the system are derived via employing Lagrange's equations of the second kind. The effect of different parameters including thickness ratio, aspect ratio, hub radius ratio and rotation speed on dimensionless natural frequencies are investigated. The dimensionless natural frequencies of CS-FEM are compared with those other existing method including the finite element method (FEM) and the assumed modes method (AMM). It is found that the CS-FEM based on Mindlin plate theory provides more accurate and "softer" solution compared with those of other methods even if using coarse meshes. In addition, the frequency loci veering phenomena associated with the mode shape interaction are examined in detail.

**Keywords:** cell-based smoothed finite element method, rotating Mindlin plate, discrete shear gap method, shear locking, natural frequencies, frequency veering.

## 1 Introduction

A lot of engineering structures consist of a flexible appendage attached to a rigid body, which are called rigid-flexible coupled structures, such as space robotic manipulators, satellite antenna, helicopter rotors, solar energy panels and aircraft engine blades and so on. Such structures can often be simplified to a rotating hub-beam or rotating-plate for dynamic analysis. Compared to the modal characteristics of non-rotating structures, those of rotating structures behave significantly, due to the coupling of the non-linear effects arising from the coupling of vibration of the flexible structure with the undergoing large rotational motions. Therefore, it is essential to conduct accurate analysis of natural frequencies and mode shapes

of these rotating structures in the design stages, considering the nonlinear effects.

The rotating structures are often idealized as rotating beams in early stage researching. The earliest works on the natural frequency of rotating beams was performed by Southwell and Gough[1] in 1921. The famous Southwell equation was presented in their work. Later, a lot of research achievement has been obtained about rotating beams [2-7]. However, there are many structures with low aspect ratios that behave like plates rather than beams. It's obvious that beam models can't obtain accurate modal characteristics and rotating plate models are more appropriate for those plate-like structures. Dokainish and Rawtani [8] used a finite element technique to determine the natural frequencies and the mode shapes of a cantilever plate mounted on the periphery of a rotating disc. The effect of the aspect ratio, the speed of rotation, the disc radius and the setting angle for the natural frequencies were discussed. Ramamurti and Kielb [9] used FEM to analyze the natural frequencies of twisted rotating plates. Yoo [10,11] used AMM to investigate the modal characteristics of a rotating cantilever plate and dimensionless parameters were identified through dimensional analysis. Hashemi [12] developed a finite element formulation for vibration analysis of rotating thick plates. The effect of different dimensionless parameters on dimensionless natural frequencies were investigated and discussed. In these references, there are two things in common: the discrete methods are FEM or AMM; the modeling theory is most based on classic plate theory (Kirchhoff plate theory), which does not work for thicker plates. Thus, more effective discrete methods based on higher order theory are necessary.

Recently, a new discrete method named smoothed FEM (S-FEM) has been proposed [13]. This method combines with the conventional FEM and the strain smoothing technique used in meshfree methods. It possesses the features of both FEM and meshfree methods. According to the different smoothing domain creation, there are a series of S-FEM models: the cell-based S-FEM (CS-FEM) [14-16], the node-based S-FEM (NS-FEM) [17-19], the edge-based S-FEM (ES-FEM) [20-22] and the face-based S-FEM (FS-FEM) [23,24], each of which has especial properties.

This paper extends the CS-FEM for non-linear free vibration analysis of a rotating plate based on Mindlin plate theory. In the present CS-FEM, we use triangular elements that can be automatically generated. The discrete shear gap (DSG) method is used to construct the strains to overcome the shear locking issue. The effectiveness of the CS-FEM is first demonstrated in some static cases and then extended for free vibration analysis of a rotating plate considering the non-linear effects arising from the coupling of vibration of the flexible structure with the undergoing large rotational motions. The effect of different parameters including thickness ratio, aspect ratio, hub radius ratio and rotation speed on dimensionless natural frequencies are investigated. The dimensionless natural frequencies of CS-FEM are compared with those other existing method including the finite element method (FEM) and the assumed modes method (AMM). It is found that the CS-FEM based on Mindlin plate theory provides "softer" solution compared with those of other methods. In addition, the frequency loci veering phenomena associated with the mode shape interaction are examined in detail.

## **2 Formulation of FEM for the Mindlin plate**

Consider a plate under bending deformation as shown in Fig.1. The middle (neutral) surface of plate is chosen as the reference plane and the problem domain. The plate is discretized with a set of three nodes triangular element as shown in Fig.2.

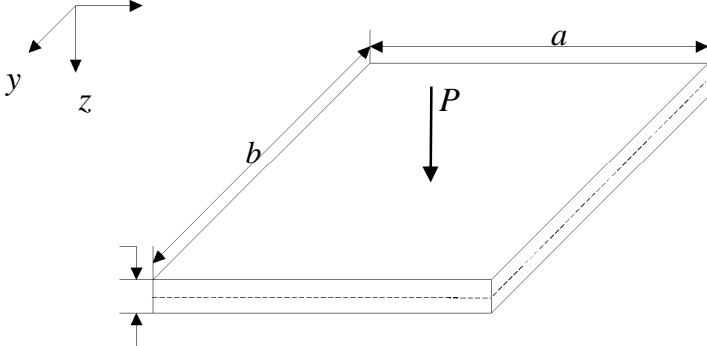


**Fig. 1 Mindlin plate with uniform thickness**

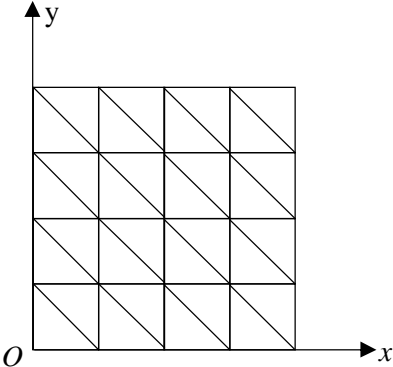


**Fig. 2 Discretization of the plate using triangular elements**

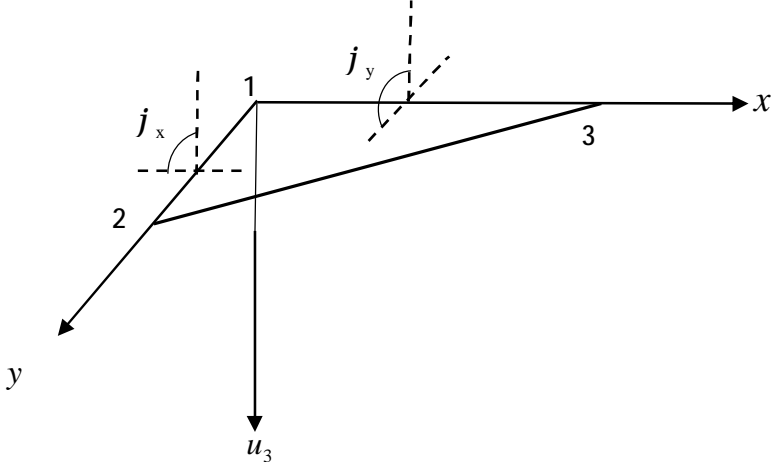


**Fig. 3 A typical three nodes triangular element**

In one triangular element as shown in Fig.3, the displacement of an arbitrary point can be expressed as

$$\mathbf{u}_e = [u_3 \quad j_x \quad j_y]^T = \sum_{i=1}^3 \begin{bmatrix} f_{3i} & 0 & 0 \\ 0 & f_{3i} & 0 \\ 0 & 0 & f_{3i} \end{bmatrix} \begin{bmatrix} u_{3i} \\ j_{xi} \\ j_{yi} \end{bmatrix} = \mathbf{f} \mathbf{d}_e \quad (1)$$

where  $u_3$  is transverse deflection, and  $j_x, j_y$  are the rotations of the middle plane around  $y$ -axis and  $x$ -axis, respectively.  $f_{3i}$  ( $i=1,2,3$ ) are the shape functions corresponding to three nodes of the triangular element and their expressions are

$$f_{3i} = a_i + b_i x + c_i y \quad (2)$$

$$\begin{cases} a_i = \frac{1}{2A_e} (x_j y_k - x_k y_j) \\ b_i = \frac{1}{2A_e} (y_j - y_k) \\ c_i = \frac{1}{2A_e} (x_k - x_j) \end{cases} \quad (3)$$

where  $A_e$  is the area of the triangular element.  $x_j$  and  $y_j$  ( $j=1,2,3$ ) are the coordinate values at the  $j$ th node. The subscript  $i, j$  and  $k$  vary from 1 to 3 and are determined by cyclic permutation in the order of  $i, j$  and  $k$ . For example, if  $i=1$ , then  $j=2, k=3$ ; or if  $i=2$ , then  $j=3, k=1$ .

The nodal displacement vector associated to node  $i$  can be expressed as  $\mathbf{d}_i = [u_{3i} \quad j_{xi} \quad j_{yi}]^T$ .

Then the bending and shear strains in the matrix forms are

$$\mathbf{z} = \sum_{i=1}^3 \mathbf{B}_i \mathbf{d}_i = \mathbf{B} \mathbf{d}_e \quad (4)$$

$$\mathbf{g} = \sum_{i=1}^3 \mathbf{S}_i \mathbf{d}_i = \mathbf{S} \mathbf{d}_e \quad (5)$$

Where

$$\mathbf{B}_i = \begin{bmatrix} 0 & f_{3i,x} & 0 \\ 0 & 0 & f_{3i,y} \\ 0 & f_{3i,y} & f_{3i,x} \end{bmatrix} \quad (6)$$

$$\mathbf{S}_i = \begin{bmatrix} f_{3i,x} & f_{3i} & 0 \\ f_{3i,y} & 0 & f_{3i} \end{bmatrix} \quad (7)$$

$$\mathbf{d}_e = [d_1 \quad d_2 \quad d_3]^T \quad (8)$$

Substituting Eq.(3) into Eq.(6) and Eq.(7), the bending strain matrix can be written as

$$\mathbf{B} = \frac{1}{2A_e} \begin{bmatrix} 0 & b-c & 0 & 0 & c & 0 & 0 & -b & 0 \\ 0 & 0 & d-a & 0 & 0 & -d & 0 & 0 & a \\ 0 & d-a & b-c & 0 & -d & c & 0 & a & -b \end{bmatrix} \quad (9)$$

$$= \frac{1}{2A_e} [\mathbf{B}_1 \quad \mathbf{B}_2 \quad \mathbf{B}_3]$$

Where

$$\begin{aligned} a &= x_2 - x_1 & b &= y_2 - y_1 \\ c &= y_3 - y_1 & d &= x_3 - x_1 \end{aligned} \quad (10)$$

As reported in many literatures, the shear locking issue often occurs when using thick plate theory to analyze thin plates. To avoid this problem, many numerical techniques have been well developed [25-30]. Recently, the discrete shear gap (DSG) method was proposed by Bletzinger *et al.* [31]. This method can be applied to both triangular and rectangular elements of different polynomial order. According to DSG method, the shear strain matrix can be written as

$$\mathbf{S} = \frac{1}{2A_e} \begin{bmatrix} b-c & A_e & 0 & c & \frac{ac}{2} & \frac{bc}{2} & -b & -\frac{bd}{2} & -\frac{bc}{2} \\ d-a & 0 & A_e & -d & -\frac{ad}{2} & -\frac{bd}{2} & a & \frac{ad}{2} & \frac{ac}{2} \end{bmatrix} \quad (11)$$

$$= \frac{1}{2A_e} [\mathbf{S}_1 \quad \mathbf{S}_2 \quad \mathbf{S}_3]$$

Then the discretized system equation of Mindlin plate with FEM for static analysis can be expressed as

$$\mathbf{K} = \int_{\Omega} \mathbf{B}^T \mathbf{D}_b \mathbf{B} d\Omega + \int_{\Omega} \mathbf{S}^T \mathbf{D}_s \mathbf{S} d\Omega \quad (12)$$

Where the matrices  $\mathbf{D}_b$  and  $\mathbf{D}_s$  are related to the bending deformation and shear deformation, respectively. They are given by

$$\mathbf{D}_b = \frac{Eh^3}{12(1-m^2)} \begin{bmatrix} 1 & m & 0 \\ m & 1 & 0 \\ 0 & 0 & \frac{(1-m)}{2} \end{bmatrix} \quad (13)$$

$$\mathbf{D}_s = \frac{kEh}{2(1+m)} \begin{bmatrix} 1 & 0 \\ 0 & 1 \end{bmatrix} \quad (14)$$

Where  $E$  is the Young's modulus,  $h$  is the thickness of the Mindlin plate,  $m$  is the Poisson's ratio and  $k$  is the shear correction factor which is given by  $k = \frac{5}{6}$ . In order to improve the accuracy of the solutions and stabilize shear force oscillations, Bischoff [32] suggested that a

stabilization term should be added to the element. Such a modification can be simply achieved by replacing  $\mathbf{D}_s$  in Eq.(14) with the following equation

$$\mathbf{D}_s = \frac{kEh^3}{2(1+m)(h^2 + ahe^2)} \begin{bmatrix} 1 & 0 \\ 0 & 1 \end{bmatrix} \quad (15)$$

Where  $h_e$  is the longest length of the edges of the element and  $a$  is a ppositive constant which is called stabilized parameter [33]. In this paper,  $a$  is fixed at 0.1.

For the free vibration analysis, the discretized system equation of Mindlin plate can be expressed as

$$(\mathbf{K} - w^2 \mathbf{M})\mathbf{d} = \mathbf{0} \quad (16)$$

Where  $w$  is the natural frequency and  $\mathbf{d}$  is the global displacement vector.  $\mathbf{M}$  is the global mass matrix and defined by

$$\mathbf{M} = \int_{\Omega} \mathbf{f}^T \mathbf{m} \mathbf{f} d\Omega = \sum_{i=1}^{N_e} \int_{\Omega_i^e} \mathbf{f}^T \mathbf{m} \mathbf{f} d\Omega_i^e \quad (17)$$

In which  $\mathbf{m}$  is a constant matrix about the mass density  $\rho$  and thickness of the plate, which is given by

$$\mathbf{m} = r \begin{bmatrix} h & 0 & 0 \\ 0 & \frac{h^3}{12} & 0 \\ 0 & 0 & \frac{h^3}{12} \end{bmatrix} \quad (18)$$

### 3 Formulation of CS-FEM for the Mindlin plate

In CS-FEM, each triangular element domain is further divided into three triangular smoothing domains by simply connecting three field nodes of the element to the central point of the element, as shown in Fig.4. These smoothing domains are not overlapping and there are no gaps between them.

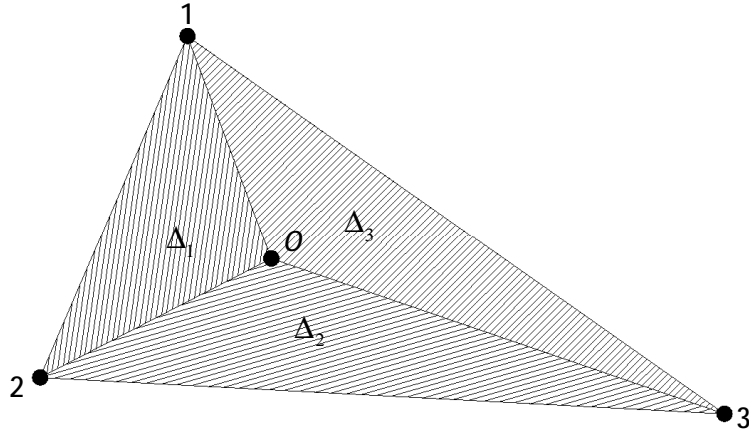


**Fig. 4 Three triangular smoothing domains**

Define the triangular element domain as  $\Omega_e$  and three triangular smoothing domains as  $\Delta_1$ ,  $\Delta_2$  and  $\Delta_3$ . Then we have  $\Omega_e = \mathbf{U}_{i=1}^3 \Delta_i$  and  $\Delta_i \cap \Delta_j = \emptyset$  ( $i \neq j$ ). The coordinates of the central point  $\mathbf{x}_o = [x_o \quad y_o]^T$  are calculated by

$$\begin{cases} x_o = \frac{1}{3}(x_1 + x_2 + x_3) \\ y_o = \frac{1}{3}(y_1 + y_2 + y_3) \end{cases} \quad (19)$$

Where  $\mathbf{x}_i = [x_i \quad y_i]^T$  with  $i=1,2,3$  are the three field nodes of the element. The displacement vector  $\mathbf{d}_o$  at the central point  $O$  is assumed to be the simple average of three displacement vectors at three field nodes of the element

$$\mathbf{d}_o = \frac{1}{3}(\mathbf{d}_1 + \mathbf{d}_2 + \mathbf{d}_3) \quad (20)$$

On the first subtriangle  $\Delta_1$  (1-2- $O$ ), the displacement of an arbitrary point in the element can be expressed as

$$\mathbf{u}_e^{\Delta_1} = \begin{bmatrix} \mathbf{f}_{31} & 0 & 0 \\ 0 & \mathbf{f}_{31} & 0 \\ 0 & 0 & \mathbf{f}_{31} \end{bmatrix} \mathbf{d}_1 + \begin{bmatrix} \mathbf{f}_{32} & 0 & 0 \\ 0 & \mathbf{f}_{32} & 0 \\ 0 & 0 & \mathbf{f}_{32} \end{bmatrix} \mathbf{d}_2 + \begin{bmatrix} \mathbf{f}_{33} & 0 & 0 \\ 0 & \mathbf{f}_{33} & 0 \\ 0 & 0 & \mathbf{f}_{33} \end{bmatrix} \mathbf{d}_o \quad (21)$$

Substituting Eq.(20) into Eq.(21), then  $\mathbf{u}_e^{\Delta_1}$  can be rewritten as

$$\mathbf{u}_e^{\Delta_1} = \left( \begin{bmatrix} \mathbf{f}_{31} & 0 & 0 \\ 0 & \mathbf{f}_{31} & 0 \\ 0 & 0 & \mathbf{f}_{31} \end{bmatrix} + \frac{1}{3} \begin{bmatrix} \mathbf{f}_{33} & 0 & 0 \\ 0 & \mathbf{f}_{33} & 0 \\ 0 & 0 & \mathbf{f}_{33} \end{bmatrix} \right) \mathbf{d}_1 + \left( \begin{bmatrix} \mathbf{f}_{32} & 0 & 0 \\ 0 & \mathbf{f}_{32} & 0 \\ 0 & 0 & \mathbf{f}_{32} \end{bmatrix} + \frac{1}{3} \begin{bmatrix} \mathbf{f}_{33} & 0 & 0 \\ 0 & \mathbf{f}_{33} & 0 \\ 0 & 0 & \mathbf{f}_{33} \end{bmatrix} \right) \mathbf{d}_2 + \frac{1}{3} \begin{bmatrix} \mathbf{f}_{33} & 0 & 0 \\ 0 & \mathbf{f}_{33} & 0 \\ 0 & 0 & \mathbf{f}_{33} \end{bmatrix} \mathbf{d}_3 \quad (22)$$

Then the strain matrices in the subtriangle  $\Delta_1$  can be obtained

$$\mathbf{z}^{\Delta_1} = \left[ \mathbf{B}_1^{\Delta_1} + \frac{1}{3} \mathbf{B}_3^{\Delta_1} \quad \mathbf{B}_2^{\Delta_1} + \frac{1}{3} \mathbf{B}_3^{\Delta_1} \quad \frac{1}{3} \mathbf{B}_3^{\Delta_1} \right] \mathbf{d}_e = \mathbf{B}^{\Delta_1} \mathbf{d}_e \quad (23)$$

$$\mathbf{g}^{\Delta_1} = \left[ \mathbf{S}_1^{\Delta_1} + \frac{1}{3} \mathbf{S}_3^{\Delta_1} \quad \mathbf{S}_2^{\Delta_1} + \frac{1}{3} \mathbf{S}_3^{\Delta_1} \quad \frac{1}{3} \mathbf{S}_3^{\Delta_1} \right] \mathbf{d}_e = \mathbf{S}^{\Delta_1} \mathbf{d}_e \quad (24)$$

Where  $\mathbf{B}^{\Delta_1}$  and  $\mathbf{S}^{\Delta_1}$  are calculated similarly as Eq.(9) and Eq.(11). The only difference is that the corresponding functions are computed in the domain of subtriangle  $\Delta_1$ , which means the three field nodes are  $\mathbf{x}_1$ ,  $\mathbf{x}_2$  and  $\mathbf{x}_o$ , respectively. Similarly, the strain matrices in the subtriangles  $\Delta_2$  (2-3-O) and  $\Delta_3$  (3-1-O) can be obtained by cyclic permutation like described in section 2. Their expressions are as follows

$$\mathbf{z}^{\Delta_2} = \left[ \frac{1}{3} \mathbf{B}_1^{\Delta_2} \quad \mathbf{B}_2^{\Delta_2} + \frac{1}{3} \mathbf{B}_1^{\Delta_2} \quad \mathbf{B}_3^{\Delta_2} + \frac{1}{3} \mathbf{B}_1^{\Delta_2} \right] \mathbf{d}_e = \mathbf{B}^{\Delta_2} \mathbf{d}_e \quad (25)$$

$$\mathbf{g}^{\Delta_2} = \left[ \frac{1}{3} \mathbf{S}_1^{\Delta_2} \quad \mathbf{S}_2^{\Delta_2} + \frac{1}{3} \mathbf{S}_1^{\Delta_2} \quad \mathbf{S}_3^{\Delta_2} + \frac{1}{3} \mathbf{S}_1^{\Delta_2} \right] \mathbf{d}_e = \mathbf{S}^{\Delta_2} \mathbf{d}_e \quad (26)$$

$$\mathbf{z}^{\Delta_3} = \left[ \mathbf{B}_1^{\Delta_3} + \frac{1}{3} \mathbf{B}_2^{\Delta_3} \quad \frac{1}{3} \mathbf{B}_2^{\Delta_3} \quad \mathbf{B}_3^{\Delta_3} + \frac{1}{3} \mathbf{B}_2^{\Delta_3} \right] \mathbf{d}_e = \mathbf{B}^{\Delta_3} \mathbf{d}_e \quad (27)$$

$$\mathbf{g}^{\Delta_3} = \left[ \mathbf{S}_1^{\Delta_3} + \frac{1}{3} \mathbf{S}_2^{\Delta_3} \quad \frac{1}{3} \mathbf{S}_2^{\Delta_3} \quad \mathbf{S}_3^{\Delta_3} + \frac{1}{3} \mathbf{S}_2^{\Delta_3} \right] \mathbf{d}_e = \mathbf{S}^{\Delta_3} \mathbf{d}_e \quad (28)$$

By applying the strain smoothing technique, the smoothed bending strain and smoothed shear strain in each triangular element can be obtained as

$$\begin{aligned} \bar{\mathbf{z}}^e &= \frac{1}{A_e} \int_{\Omega_e} \mathbf{z}(x, y) d\Omega_e \\ &= \frac{1}{A_e} \left( \int_{\Delta_1} \mathbf{z}^{\Delta_1} d\Delta_1 + \int_{\Delta_2} \mathbf{z}^{\Delta_2} d\Delta_2 + \int_{\Delta_3} \mathbf{z}^{\Delta_3} d\Delta_3 \right) \end{aligned} \quad (29)$$

$$\begin{aligned}\mathbf{g}_e^0 &= \frac{1}{A_e} \int_{\Omega_e} \mathbf{g}(x, y) d\Omega_e \\ &= \frac{1}{A_e} \left( \int_{\Delta_1} \mathbf{g}^{\Delta_1} d\Delta_1 + \int_{\Delta_2} \mathbf{g}^{\Delta_2} d\Delta_2 + \int_{\Delta_3} \mathbf{g}^{\Delta_3} d\Delta_3 \right)\end{aligned}\quad (30)$$

Because the strain in the subtriangles are constant, Eq.(29) and Eq.(30) can be rewritten as

$$\mathbf{z}_e^0 = \frac{A_{\Delta_1} \mathbf{z}^{\Delta_1} + A_{\Delta_2} \mathbf{z}^{\Delta_2} + A_{\Delta_3} \mathbf{z}^{\Delta_3}}{A_e} = \mathbf{B}_e^0 \mathbf{u}_e \quad (31)$$

$$\mathbf{g}_e^0 = \frac{A_{\Delta_1} \mathbf{g}^{\Delta_1} + A_{\Delta_2} \mathbf{g}^{\Delta_2} + A_{\Delta_3} \mathbf{g}^{\Delta_3}}{A_e} = \mathbf{S}_e^0 \mathbf{u}_e \quad (32)$$

Where the smoothed strain matrices are as follows

$$\mathbf{B}_e^0 = \frac{A_{\Delta_1} \mathbf{B}^{\Delta_1} + A_{\Delta_2} \mathbf{B}^{\Delta_2} + A_{\Delta_3} \mathbf{B}^{\Delta_3}}{A_e} \quad (33)$$

$$\mathbf{S}_e^0 = \frac{A_{\Delta_1} \mathbf{S}^{\Delta_1} + A_{\Delta_2} \mathbf{S}^{\Delta_2} + A_{\Delta_3} \mathbf{S}^{\Delta_3}}{A_e} \quad (34)$$

In which  $A_e$  is the area of triangular element.  $A_{\Delta_1}$ ,  $A_{\Delta_2}$  and  $A_{\Delta_3}$  are the areas of three subtriangles, respectively. Substituting Eqs.(33) and (34) into Eq.(12), the smoothed element stiffness matrix can be given by

$$\mathbf{K}_e^0 = \int_{\Omega_e} \mathbf{B}_e^{0T} \mathbf{D}_b \mathbf{B}_e^0 d\Omega_e + \int_{\Omega_e} \mathbf{S}_e^{0T} \mathbf{D}_s \mathbf{S}_e^0 d\Omega_e \quad (35)$$

Where the matrices  $\mathbf{D}_b$  and  $\mathbf{D}_s$  are the same as Eqs.(13) and (15). Then the global stiffness matrix of the CS-FEM can be assembled by

$$\hat{\mathbf{K}} = \sum_{e=1}^{N_e} \mathbf{K}_e^0 \quad (36)$$

It should be mentioned that the central point in each element is only used to form the smoothing domain. Finally, the displacement vector of this point will be replaced by those of three field nodes of the element as shown in Eq.(22). Hence, there are no extra DOFs, which means the DOFs of CS-FEM are the same as FEM if using the same mesh.

## 4 Nonlinear dynamic equations of rotating plates based on Mindlin plate theory

### 4.1 Dynamic equations of a Mindlin plate undergoing overall motion

In Mindlin plate theory, the plate doesn't demand the cross section be perpendicular to the neutral plane after deformation. The transverse shear strain which is neglected in classical thin plate theory is taken into account. In this section, the nonlinear dynamic equations of a rotating rectangular Mindlin plate undergoing overall motion in three-dimensional space will be presented in detail.

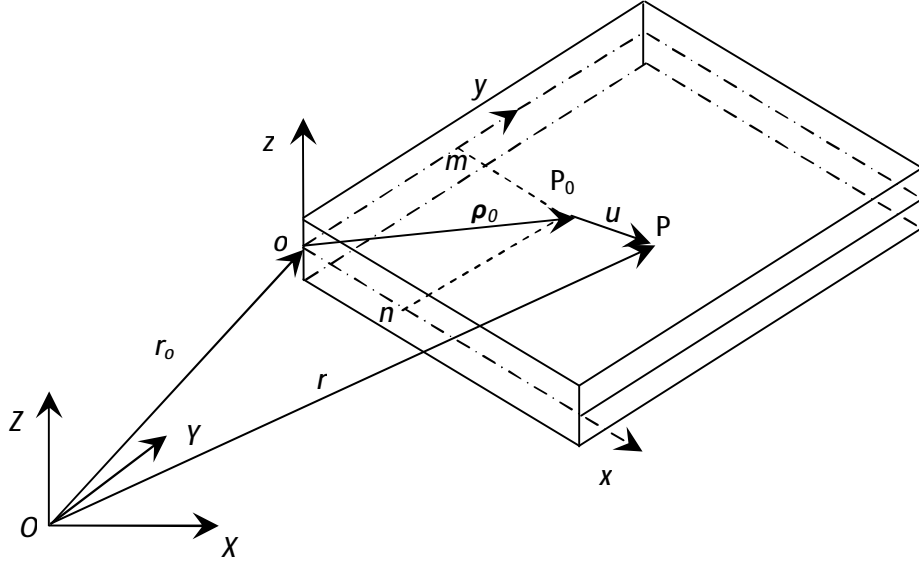


**Fig. 5 The configuration of a rectangular Mindlin plate**

Consider a flexible plate undergoing overall motion as shown in Fig.5. The inertial coordinate system and the local coordinate system which is fixed to the neutral surface of the plate are denoted by  $O-XYZ$  and  $o-xyz$ , respectively. The physical parameters of the plate are as follows: length  $a$ , width  $b$ , thickness  $h$ , Young's modulus  $E$ , mass density  $\rho$  and Poisson's ratio  $\mu$ .  $P_0$  is an arbitrary point on the undeformed neutral surface of the plate in the local coordinate system. After deformation, it moves to  $P$  and the displacement vector is denoted by  $\mathbf{u} = (u_1, u_2, u_3)^T$  where  $u_1$ ,  $u_2$  and  $u_3$  are the displacement components along the  $x$ ,  $y$  and  $z$  axis in the local coordinate system, respectively. The displacement components  $u_1$  and  $u_2$  can be expressed as

$$\begin{cases} u_1 = w_1 - \frac{1}{2} \int_0^x \left( \frac{\partial u_3}{\partial x} \right)^2 dx + z j_x \\ u_2 = w_2 - \frac{1}{2} \int_0^y \left( \frac{\partial u_3}{\partial y} \right)^2 dy + z j_y \end{cases} \quad (37)$$

Where  $w_1$  and  $w_2$  are neutral surface stretch along the  $x$  and  $y$  axis, respectively.

$-\frac{1}{2} \int_0^x \left( \frac{\partial u_3}{\partial x} \right)^2 dx$  and  $-\frac{1}{2} \int_0^y \left( \frac{\partial u_3}{\partial y} \right)^2 dy$  are the coupling terms of the deformation which are caused the transverse deformation. In the traditional approximate model, these two coupling terms are ignored because of the small deformation assumption.  $j_x$  and  $j_y$  are the rotations of the middle plane around  $y$ -axis and  $x$ -axis, respectively. The velocity vector of an arbitrary point  $P$  in the inertial coordinate system can be expressed as

$$\mathbf{V}_P = \mathbf{V}_o + \boldsymbol{\omega}_A \times (\boldsymbol{\rho}_0 + \mathbf{u}) + \mathbf{V}^{PA} \quad (38)$$

Where  $\mathbf{V}_o$  and  $\boldsymbol{\omega}_A$  are the velocity and angular velocity of the local coordinate system relative

to the inertial coordinate system, respectively.  $\rho_0$  and  $V^{PA}$  are the position vector of point  $P_0$  and the velocity vector of point  $P$  in the local coordinate system, respectively. These vectors are as follows

$$V_o = v_1 e_1 + v_2 e_2 + v_3 e_3 \quad \omega_A = w_1 e_1 + w_2 e_2 + w_3 e_3 \quad (39)$$

$$\rho_0 = x e_1 + y e_2 \quad u = u_1 e_1 + u_2 e_2 + u_3 e_3 \quad V_{PA} = u_1 e_1 + u_2 e_2 + u_3 e_3 \quad (40)$$

Where  $e_1$ ,  $e_2$  and  $e_3$  are the unit vectors along  $x$ ,  $y$ , and  $z$  axis, respectively. Substituting Eqs.(39) and (40) into Eq.(38), the velocity vector of an arbitrary point  $P$  in the inertial coordinate system can be obtained as

$$V_P = [v_1 + u_1 w_1 + w_2 u_3 - w_3 (y + u_2)] e_1 + [v_2 + u_2 w_2 + w_3 (x + u_1) - w_1 u_3] e_2 + [v_3 + u_3 w_3 + w_1 (y + u_2) - w_2 (x + u_1)] e_3 \quad (41)$$

Then the kinetic energy of the system is

$$T = \frac{1}{2} \int_V r V_P^T V_P dV = \frac{1}{2} \iint_A r h V_P^T V_P dA \quad (42)$$

According to Mindlin plate theory, the strain vectors can be obtained as

$$e = \begin{cases} e_{xx} = \frac{\partial w_1}{\partial x} + z \frac{\partial j_x}{\partial x} \\ e_{yy} = \frac{\partial w_2}{\partial y} + z \frac{\partial j_y}{\partial y} \\ g_{xy} \approx \frac{\partial w_1}{\partial y} + \frac{\partial w_2}{\partial x} + z \left( \frac{\partial j_x}{\partial y} + \frac{\partial j_y}{\partial x} \right) \\ g_{xz} = \frac{\partial u_3}{\partial x} + j_x \\ g_{yz} = \frac{\partial u_3}{\partial y} + j_y \end{cases} \quad (43)$$

Compared to the Kirchhoff plate theory, the strain components  $g_{xz}$  and  $g_{yz}$  are not equal zero.

Then the stress vectors for isotropic materials are obtained as

$$s = \frac{E}{1-m^2} \begin{bmatrix} 1 & m & 0 & 0 & 0 \\ m & 1 & 0 & 0 & 0 \\ 0 & 0 & (1-m)/2 & 0 & 0 \\ 0 & 0 & 0 & k(1-m)/2 & 0 \\ 0 & 0 & 0 & 0 & k(1-m)/2 \end{bmatrix} \begin{bmatrix} e_{xx} \\ e_{yy} \\ g_{xy} \\ g_{xz} \\ g_{yz} \end{bmatrix} \quad (44)$$

Where  $k$  is the shear correction factor which is given by  $k = \frac{5}{6}$ . Now the total potential energy of the system is as follows

$$\begin{aligned}
U &= \frac{1}{2} \iiint_V \mathbf{e}^T \mathbf{S} dV \\
&= \frac{1}{2} \iiint_V \frac{E}{1-m^2} (\mathbf{e}_{xx}^2 + 2m \mathbf{e}_{xx} \mathbf{e}_{yy} + \mathbf{e}_{yy}^2 + \frac{1-m}{2} \mathbf{g}_{xy}^2 + \frac{k(1-m)}{2} \mathbf{g}_{xz}^2 + \frac{k(1-m)}{2} \mathbf{g}_{yz}^2) dV \quad (45) \\
&= U_1 + U_2
\end{aligned}$$

Where  $U_1$  represents the bending strain energy and  $U_2$  represents the in-plane strain energy of the plate. They can be denoted as

$$\begin{aligned}
U_1 &= \frac{1}{2} \iint_A \left\{ \frac{Eh}{1-m^2} \left[ \left( \frac{\partial w_1}{\partial x} \right)^2 + \left( \frac{\partial w_2}{\partial y} \right)^2 + 2m \left( \frac{\partial w_1}{\partial x} \right) \left( \frac{\partial w_2}{\partial y} \right) \right] + \frac{Eh}{2(1+m)} \left( \frac{\partial w_1}{\partial y} + \frac{\partial w_2}{\partial x} \right)^2 \right\} dA \quad (46) \\
U_2 &= \frac{Eh^3}{24(1-m^2)} \iint_A \left[ \left( \frac{\partial^2 j_x}{\partial x^2} \right)^2 + \left( \frac{\partial^2 j_y}{\partial y^2} \right)^2 + 2m \left( \frac{\partial j_x}{\partial x} \right) \left( \frac{\partial j_y}{\partial y} \right) + \frac{1-m}{2} \left( \frac{\partial j_x}{\partial y} + \frac{\partial j_y}{\partial x} \right)^2 \right] dA \\
&\quad + \frac{kEh}{4(1+m)} \iint_A \left[ \left( \frac{\partial u_3}{\partial x} + j_x \right)^2 + \left( \frac{\partial u_3}{\partial y} + j_y \right)^2 \right] dA \quad (47)
\end{aligned}$$

Discretize the plate using triangular elements as shown in Fig.2. The unknown deformation variables can be expressed as

$$\left\{ \begin{aligned}
w_1(x, y, t) &= \sum_{i=1}^3 f_{1i}(x, y) q_{1i}(t) = \mathbf{f}_1(x, y) \mathbf{q}_1(t) \\
w_2(x, y, t) &= \sum_{i=1}^3 f_{2i}(x, y) q_{2i}(t) = \mathbf{f}_2(x, y) \mathbf{q}_2(t) \\
u_3(x, y, t) &= \sum_{i=1}^3 f_{3i}(x, y) q_{3i}(t) = \mathbf{F}_3(x, y) \mathbf{q}_3(t) \\
j_x(x, y, t) &= \sum_{i=1}^3 f_{4i}(x, y) q_{3i}(t) = \mathbf{f}_4(x, y) \mathbf{q}_3(t) \\
j_y(x, y, t) &= \sum_{i=1}^3 f_{5i}(x, y) q_{3i}(t) = \mathbf{f}_5(x, y) \mathbf{q}_3(t)
\end{aligned} \right. \quad (48)$$

Where  $\mathbf{f}_{1i}(x, y)$ ,  $\mathbf{f}_{2i}(x, y)$ ,  $\mathbf{f}_{3i}$ ,  $\mathbf{f}_{4i}$  and  $\mathbf{f}_{5i}$  are shape functions in one element corresponding to the node  $i$ .  $\mathbf{q}_i(t)$  ( $i=1,2,3$ ) are generalized coordinates. Let  $\mathbf{F}_4 = z\mathbf{f}_4$  and  $\mathbf{F}_5 = z\mathbf{f}_5$ , then substituting them into Eq.(37), we can have the displacement and velocity components

$$\left\{ \begin{aligned}
u_1 &= \mathbf{f}_1 \mathbf{q}_1 - \frac{1}{2} \mathbf{q}_3^T \mathbf{H}_1(x, y) \mathbf{q}_3 + \mathbf{F}_4 \mathbf{q}_3 \\
u_2 &= \mathbf{f}_2 \mathbf{q}_2 - \frac{1}{2} \mathbf{q}_3^T \mathbf{H}_2(x, y) \mathbf{q}_3 + \mathbf{F}_5 \mathbf{q}_3
\end{aligned} \right. \quad (49)$$

$$\left\{ \begin{aligned}
\dot{\mathbf{u}}_1 &= \mathbf{f}_1 \dot{\mathbf{q}}_1 - \mathbf{q}_3^T \mathbf{H}_1(x, y) \dot{\mathbf{q}}_3 + \mathbf{F}_4 \dot{\mathbf{q}}_3 \\
\dot{\mathbf{u}}_2 &= \mathbf{f}_2 \dot{\mathbf{q}}_2 - \mathbf{q}_3^T \mathbf{H}_2(x, y) \dot{\mathbf{q}}_3 + \mathbf{F}_5 \dot{\mathbf{q}}_3
\end{aligned} \right. \quad (50)$$

Where  $\mathbf{H}_1(x, y)$  and  $\mathbf{H}_2(x, y)$  are coupling shape functions which are defined by

$$\begin{cases} \mathbf{H}_1 = \mathbf{R}_{j_3}^T \int_{x_{jl}}^x \mathbf{f}_{3,x}^T \mathbf{f}_{3,x} dx \mathbf{R}_{j_3} + \sum_{i \in mP_0} \mathbf{R}_{i_3}^T \int_{x_{ik}}^{x_{il}} \mathbf{f}_{3,x}^T \mathbf{f}_{3,x} dx \mathbf{R}_{i_3} \\ \mathbf{H}_2 = \mathbf{R}_{j_3}^T \int_{y_{jl}}^y \mathbf{f}_{3,y}^T \mathbf{f}_{3,y} dy \mathbf{R}_{j_3} + \sum_{i \in nP_0} \mathbf{R}_{i_3}^T \int_{y_{il}}^{y_{il}} \mathbf{f}_{3,y}^T \mathbf{f}_{3,y} dy \mathbf{R}_{i_3} \end{cases} \quad (51)$$

If these coupling terms are neglected, the results will be divergent when the angular velocity is high. There will be a so-called dynamic stiffening problem [34]. In Eq.(51),  $\mathbf{R}_{j_3}$  is the orientation matrix decided by nodal numbering of the element. The comma means the first shape derivative of shape function versus  $x$  or  $y$ .  $mP_0$  and  $nP_0$  denote the collection of elements through these two segments.

Let  $\mathbf{q} = [\mathbf{q}_1^T, \mathbf{q}_2^T, \mathbf{q}_3^T]^T$  be the generalized coordinate vector. Substituting Eqs.(42) and (45) into Lagrange's equations of the second kind

$$\frac{d}{dt} \left( \frac{\partial T}{\partial \dot{\mathbf{q}}} \right) - \frac{\partial T}{\partial \mathbf{q}} + \frac{\partial U}{\partial \mathbf{q}} = \mathbf{0} \quad (52)$$

Then the strong-coupled and nonlinear dynamic equations of the plate undergoing overall motion can be given by

$$\begin{bmatrix} \mathbf{M}_{11} & \mathbf{0} & \mathbf{M}_{13} \\ \mathbf{0} & \mathbf{M}_{22} & \mathbf{M}_{23} \\ \mathbf{M}_{31} & \mathbf{M}_{32} & \mathbf{M}_{33} \end{bmatrix} \begin{bmatrix} \ddot{\mathbf{q}}_1 \\ \ddot{\mathbf{q}}_2 \\ \ddot{\mathbf{q}}_3 \end{bmatrix} + \begin{bmatrix} \mathbf{0} & \mathbf{G}_{12} & \mathbf{G}_{13} \\ \mathbf{G}_{21} & \mathbf{0} & \mathbf{G}_{23} \\ \mathbf{G}_{31} & \mathbf{G}_{32} & \mathbf{G}_{33} \end{bmatrix} \begin{bmatrix} \dot{\mathbf{q}}_1 \\ \dot{\mathbf{q}}_2 \\ \dot{\mathbf{q}}_3 \end{bmatrix} + \begin{bmatrix} \mathbf{K}_{11} & \mathbf{K}_{12} & \mathbf{K}_{13} \\ \mathbf{K}_{21} & \mathbf{K}_{22} & \mathbf{K}_{23} \\ \mathbf{K}_{31} & \mathbf{K}_{32} & \mathbf{K}_{33} \end{bmatrix} \begin{bmatrix} \mathbf{q}_1 \\ \mathbf{q}_2 \\ \mathbf{q}_3 \end{bmatrix} = \begin{bmatrix} \mathbf{Q}_1 \\ \mathbf{Q}_2 \\ \mathbf{Q}_3 \end{bmatrix} \quad (53)$$

Where

$$\mathbf{M}_{11} = \mathbf{W}_{11}, \quad \mathbf{M}_{22} = \mathbf{W}_{22}, \quad \mathbf{M}_{33} = \mathbf{W}_{33} + \mathbf{W}_{44} + \mathbf{W}_{55} \quad (54)$$

$$\mathbf{M}_{31} = \mathbf{M}_{13}^T = \mathbf{W}_{41}, \quad \mathbf{M}_{32} = \mathbf{M}_{23}^T = \mathbf{W}_{52} \quad (55)$$

$$\mathbf{G}_{12} = -\mathbf{G}_{21}^T = -2w_3 \mathbf{W}_{12}, \quad \mathbf{G}_{23} = -\mathbf{G}_{32}^T = -2w_1 \mathbf{W}_{23} \quad (56)$$

$$\mathbf{G}_{13} = -\mathbf{G}_{31}^T = 2(w_2 \mathbf{W}_{13} - w_3 \mathbf{W}_{15}) \quad (57)$$

$$\mathbf{G}_{33} = 2w_2 (\mathbf{W}_{43} - \mathbf{W}_{34}) + 2w_3 (\mathbf{W}_{54} - \mathbf{W}_{45}) + 2w_1 (\mathbf{W}_{35} - \mathbf{W}_{53}) \quad (58)$$

$$\mathbf{K}_{11} = \mathbf{K}_{f11} - (w_2^2 + w_3^2) \mathbf{W}_{11}, \quad \mathbf{K}_{12} = \mathbf{K}_{f12} + (w_1 w_2 - w_3) \mathbf{W}_{12} \quad (59)$$

$$\mathbf{K}_{13} = (w_1 w_3 + w_2) \mathbf{W}_{13} - (w_2^2 + w_3^2) \mathbf{W}_{14} + (w_1 w_2 - w_3) \mathbf{W}_{15} \quad (60)$$

$$\mathbf{K}_{21} = \mathbf{K}_{f21} + (w_1 w_2 + w_3) \mathbf{W}_{21}, \quad \mathbf{K}_{22} = \mathbf{K}_{f22} - (w_1^2 + w_3^2) \mathbf{W}_{22} \quad (61)$$

$$\mathbf{K}_{23} = (w_2 w_3 - w_1) \mathbf{W}_{23} + (w_3 + w_1 w_2) \mathbf{W}_{24} - (w_1^2 + w_3^2) \mathbf{W}_{25} \quad (62)$$

$$\mathbf{K}_{31} = (w_1 w_3 - w_2) \mathbf{W}_{31} - (w_2^2 + w_3^2) \mathbf{W}_{41} + (w_1 w_2 + w_3) \mathbf{W}_{51} \quad (63)$$

$$\mathbf{K}_{32} = (w_2 w_3 + \mathbf{i}\mathbf{k})\mathbf{W}_{32} + (w_1 w_2 - \mathbf{i}\mathbf{k})\mathbf{W}_{42} - (w_1^2 + w_3^2)\mathbf{W}_{52} \quad (64)$$

$$\begin{aligned} \mathbf{K}_{33} = & \mathbf{K}_{f33} - (w_1^2 + w_2^2)\mathbf{W}_{33} - (w_2^2 + w_3^2)\mathbf{W}_{44} - (w_1^2 + w_3^2)\mathbf{W}_{55} - \mathbf{i}\mathbf{k}\mathbf{W}_{34} + \mathbf{i}\mathbf{k}\mathbf{W}_{35} \\ & + (2w_1 w_3 + \mathbf{i}\mathbf{k})\mathbf{W}_{43} + (2w_1 w_2 - \mathbf{i}\mathbf{k})\mathbf{W}_{45} + (2w_2 w_3 - \mathbf{i}\mathbf{k})\mathbf{W}_{53} + \mathbf{i}\mathbf{k}\mathbf{W}_{54} \\ & + \underline{(w_2^2 + w_3^2)\mathbf{D}_{11} + (w_1^2 + w_3^2)\mathbf{D}_{22} - (w_1 w_2 + \mathbf{i}\mathbf{k})\mathbf{D}_{12} - (w_1 w_2 - \mathbf{i}\mathbf{k})\mathbf{D}_{21} - a_{01}\mathbf{C}_1 - a_{02}\mathbf{C}_2} \end{aligned} \quad (65)$$

$$\mathbf{Q}_1 = (w_2^2 + w_3^2)\mathbf{S}_{11}^T - (w_1 w_2 - \mathbf{i}\mathbf{k})\mathbf{S}_{21}^T - a_{01}\mathbf{Y}_1^T \quad (66)$$

$$\mathbf{Q}_2 = (w_1^2 + w_3^2)\mathbf{S}_{22}^T - (w_1 w_2 + \mathbf{i}\mathbf{k})\mathbf{S}_{12}^T - a_{02}\mathbf{Y}_2^T \quad (67)$$

$$\begin{aligned} \mathbf{Q}_3 = & -(w_1 w_3 - \mathbf{i}\mathbf{k})\mathbf{S}_{13}^T + (w_2^2 + w_3^2)\mathbf{S}_{14}^T - (w_1 w_2 + \mathbf{i}\mathbf{k})\mathbf{S}_{15}^T - (w_2 w_3 + \mathbf{i}\mathbf{k})\mathbf{S}_{23}^T \\ & - (w_1 w_2 - \mathbf{i}\mathbf{k})\mathbf{S}_{24}^T + (w_1^2 + w_3^2)\mathbf{S}_{25}^T - a_{03}\mathbf{Y}_3^T - a_{01}\mathbf{Y}_4^T - a_{02}\mathbf{Y}_5^T \end{aligned} \quad (68)$$

In which  $a_{01}$ ,  $a_{02}$  and  $a_{03}$  are the acceleration of point  $O$  in the local coordinate system which are denoted as

$$a_{01} = \mathbf{k} + (w_2 v_3 - w_3 v_2) \quad a_{02} = \mathbf{k} + (w_3 v_1 - w_1 v_3) \quad a_{03} = \mathbf{k} + (w_1 v_2 - w_2 v_1) \quad (69)$$

The constant matrices in Eq.(53) are defined by

$$\mathbf{W}_{ij} = \iiint_V r \mathbf{F}_i^T \mathbf{F}_j dV \quad (i=1, \mathbf{L}, 5; j=1, \mathbf{L}, 5) \quad (70)$$

$$\mathbf{C}_i = \iint_A r h \cdot \mathbf{H}_i dA \quad (i=1, 2) \quad (71)$$

$$\mathbf{D}_{1i} = \iint_A r h \cdot x \cdot \mathbf{H}_i dA \quad (i=1, 2) \quad (72)$$

$$\mathbf{D}_{2i} = \iint_A r h \cdot y \cdot \mathbf{H}_i dA \quad (i=1, 2) \quad (73)$$

$$\mathbf{S}_{1i} = \iiint_V r x \mathbf{F}_i dV \quad (i=1, \mathbf{L}, 5) \quad (74)$$

$$\mathbf{S}_{2i} = \iiint_V r y \mathbf{F}_i dV \quad (i=1, \mathbf{L}, 5) \quad (75)$$

$$\mathbf{Y}_i = \iiint_V r \mathbf{F}_i dV \quad (i=1, \mathbf{L}, 5) \quad (76)$$

$$\mathbf{K}_{f11} = \iint_A \frac{Eh}{1-m^2} (\mathbf{F}_{1,x}^T \mathbf{F}_{1,x} + \frac{1-m}{2} \mathbf{F}_{1,y}^T \mathbf{F}_{1,y}) dA \quad (77)$$

$$\mathbf{K}_{f12} = \mathbf{K}_{f21}^T = \iint_A \frac{Eh}{1-m^2} (m \mathbf{F}_{1,x}^T \mathbf{F}_{2,y} + \frac{1-m}{2} \mathbf{F}_{1,y}^T \mathbf{F}_{2,x}) dA \quad (78)$$

$$\mathbf{K}_{f22} = \iint_A \frac{Eh}{1-m^2} (\mathbf{F}_{2,y}^T \mathbf{F}_{2,y} + \frac{1-m}{2} \mathbf{F}_{2,x}^T \mathbf{F}_{2,x}) dA \quad (79)$$

$$\begin{aligned}
\mathbf{K}_{f33} = & \iint_A \frac{Eh^3}{12(1-m^2)} [F_{4,x}^T F_{4,x} + F_{5,y}^T F_{5,y} + m(F_{4,x}^T F_{5,y} + F_{5,y}^T F_{4,x}) \\
& + \frac{1-m}{2} (F_{4,y}^T F_{4,y} + F_{5,x}^T F_{5,x} + F_{4,y}^T F_{5,x} + F_{5,x}^T F_{4,y})] dA \\
& + \frac{kEh}{2(1+m)} \iint_A [F_{3,x}^T F_{3,x} + F_{3,y}^T F_{3,y} + F_4^T F_4 + F_5^T F_5 \\
& + F_{3,x}^T F_4 + F_4^T F_{3,x} + F_{3,y}^T F_5 + F_5^T F_{3,y}] dA
\end{aligned} \tag{80}$$

Nonlinear dynamic equation (53) can be used not only for the analysis of thin plates, but also for the analysis of thick plates. These underlined terms in Eq.(65) are additional dynamic stiffness terms which are caused by considering the coupling shape functions. If these coupling terms are neglected, the results will be divergent when the angular velocity is high which is mentioned in reference [34].

#### 4.2 Formulation for vibration analysis of a rotating cantilever Mindlin plate

Consider a flexible plate attached to a rigid hub with radius  $R$ , and rotating around the  $y$  axis with a constant rotation speed  $W$  in the local coordinate system  $xyz$  which is fixed to the neutral surface of the plate as shown in Fig.5. The physical parameters of the plate are as follows: length  $a$ , width  $b$ , thickness  $h$ , Young's modulus  $E$ , mass density  $\rho$  and Poisson's ratio  $\mu$ .

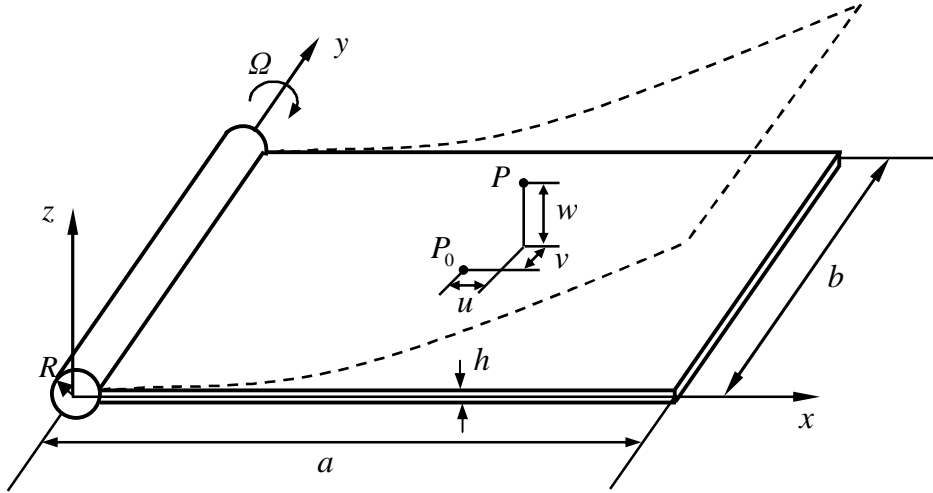


**Fig. 6 The configuration of a rotating cantilever Mindlin plate**

In the local coordinate system  $xyz$ , the velocity and angular velocity of point  $O$  in the direction of  $x$ ,  $y$ , and  $z$  axis are

$$v_1 = v_2 = 0, v_3 = -RW, w_1 = w_3 = 0, w_2 = W \tag{81}$$

Ignoring the in-plane motions of the plate and the right-hand side terms in Eq.(53), the dynamic equation for the free vibration analysis of the rotating plate can be obtained as

$$\mathbf{M}_{33} \ddot{\mathbf{q}}_3 + [\underline{W^2(RC_1 + D_{11})} - W^2(W_{33} + W_{44}) + \mathbf{K}_{f33}] \mathbf{q}_3 = \mathbf{0} \tag{82}$$

Note that the underlined term is the dynamic stiffness term due to rotation, the second term is

the dynamic softness term and the last term is the static stiffness term. Rewrite Eq.(82) in a non-dimensional form. The following non-dimensional variables are defined:

$$d = \frac{a}{b}, \quad h = \frac{h}{a}, \quad s = \frac{R}{a}, \quad v = wT, \quad g = WT \quad (83)$$

Where  $T = \sqrt{rha^4 / D}$ . Then Eq.(82) can be rewritten in the non-dimensional form:

$$\bar{M}_{33} \ddot{\mathbf{q}}_3 + [W^2(R\bar{C}_1 + \bar{D}_{11}) - W^2(\bar{W}_{33} + \bar{W}_{44}) + \bar{K}_{f33}] \mathbf{q}_3 = \mathbf{0} \quad (84)$$

Their expressions can be found in Eqs.(70),(71),(72) and (80). The difference is that the integration of constant matrices is from 0 to 1 in Eq.(84).

## 5 Numerical results

### 5.1 Elimination of shear locking

To examine the efficiency of CS-FEM for static deflection analyses, consider a rectangular plate with uniform load  $f=1\text{N/m}^2$  as shown in Fig.1. The geometric and material property parameters are as follows:  $a=10.0\text{m}$ ,  $b=10.0\text{m}$ ,  $E=1.0 \times 10^9 \text{N/m}^2$  and  $m=0.3$ . Define a deflection coefficient  $x = w_{\max} D / fb^4$ , where  $w_{\max}$  is the maximum deflection at the center of

the plate and the elastic rigidity of the plate is  $D = \frac{Eh^3}{12(1-m^2)}$ .

Table 1 shows the deflection coefficient of the clamped plate against the different mesh densities  $N \times N$  for the thin plate (aspect ratio  $h/a=0.001$ ) and thick plate (aspect ratio  $h/a=0.1$ ). It is seen that the CS-FEM and FEM with DSG method both provide a locking-free solution. The plate is meshed by more elements, the results will be more accurate. In addition, the results of CS-FEM are more accurate and softer than those of FEM with the same DOFs for both thin and thick plates. The deflection coefficient of the simply supported plate against the different mesh densities  $N \times N$  for the thin plate (aspect ratio  $h/a=0.001$ ) and thick plate (aspect ratio  $h/a=0.1$ ) is presented in Table2. The same comments as in the clamped plate can be obtained again.

**Table 1 The deflection coefficient of the clamped plate**

$h/a$	Method	Mesh densities $N \times N$					Analytical solutions[35]
		$4 \times 4$	$8 \times 8$	$10 \times 10$	$16 \times 16$	$20 \times 20$	
0.001	FEM	0.000906	0.001121	0.001167	0.001225	0.001239	0.001266
	CS-FEM	0.001123	0.001227	0.001241	0.001256	0.001259	
	FEM	0.001203	0.001425	0.001456	0.001487	0.001493	
0.1	CS-FEM	0.001357	0.001467	0.001480	0.001495	0.001498	0.001499
	FEM						

**Table 2 The deflection coefficient of the simply supported plate**

$h/a$	Method	Mesh densities $N \times N$					Analytical solutions[35]
		$4 \times 4$	$8 \times 8$	$10 \times 10$	$16 \times 16$	$20 \times 20$	
0.001	FEM	0.002949	0.003728	0.003844	0.003975	0.004006	0.004062
	CS-FEM	0.003517	0.003928	0.003977	0.004030	0.004042	
	FEM	0.003349	0.004058	0.004142	0.004225	0.004243	
0.1	CS-FEM	0.003748	0.004143	0.004190	0.004240	0.004252	0.004273
	FEM						

### 5.2 Free vibration analysis of the plate with different boundary conditions

Consider a rectangular plate as shown in Fig.1. The geometric and material property parameters are as follows:  $a=10.0\text{m}$  ,  $b=10.0\text{m}$  ,  $E=2.0 \times 10^{11} \text{ N/m}^2$  ,  $r=8000 \text{ kg/m}^3$  and

$m=0.3$ . Define a dimensionless frequency coefficient  $\nu=(w^2 r a^4 h / D)^{1/4}$ , where  $w$  is the natural frequency and  $D$  is the elastic rigidity of the plate which is the same as mentioned in last section. The combined boundary condition is defined by different symbols. The symbols F, S and C represent the free, simply supported and clamped boundary conditions, respectively. For example, SFCF means a combined boundary condition for a plate whose four edges are simply supported, free, clamped and free. In order to get more accurate results [36], the well-known lumped mass matrix is used in this paper.

Tables 3 and 4 show the six lowest dimensionless frequencies of thin plate (aspect ratio  $h/a=0.005$ ) and thick plate (aspect ratio  $h/a=0.1$ ) with SSSS boundary condition. It is seen that the results of the CS-FEM agree well with the results of reference [37]. For the thin plate, there is no shear locking phenomenon because of using DSG method. The results of CS-FEM are more accurate than those of FEM with the same DOFs. In particular, the CS-FEM can provide accurately values of frequencies even if using coarse meshes. Tables 5 and 6 show the six lowest dimensionless frequencies of thin plate (aspect ratio  $h/a=0.005$ ) and thick plate (aspect ratio  $h/a=0.1$ ) with CCCC boundary condition and the obtained comments in the SSSS plate are confirmed for the CCCC plate again. The other five different boundary conditions: SSSF, SFSE, CCFE, CFCE and CFSF for thin plate (aspect ratio  $h/a=0.005$ ) are listed in Table 7. The plate is discretized with  $2 \times 16 \times 16$  triangular elements. It is again observed that the results of CS-FEM agree well with the results of reference. The six lowest shape modes of thin plate (aspect ratio  $h/a=0.005$ ) with SSSS boundary condition are plotted in Fig.7. It is seen that they express exactly the real physical modes and there is no spurious energy modes are found.

**Table 3 The dimensionless frequency coefficient  $\nu$  of a SSSS plate ( $h/a=0.005$ )**

Mesh	Method	Mode number					
		1	2	3	4	5	6
$4 \times 4$	FEM	4.9382	7.8786	8.9396	10.5890	12.2902	12.9570

	CS-FEM	4.4965	7.1241	7.2503	9.0931	10.0933	10.1619
8×8	FEM	4.5708	7.2889	7.5694	9.6691	10.8368	11.0471
	CS-FEM	4.4543	7.0536	7.0791	8.9750	10.0418	10.0477
16×16	FEM	4.4745	7.0941	7.1603	9.1230	10.1731	10.1872
	CS-FEM	4.4453	7.0310	7.0367	8.9051	9.9590	9.9592
20×20	FEM	4.4629	7.0691	7.1108	9.0396	10.0871	10.0928
	CS-FEM	4.4443	7.0284	7.0320	8.8972	9.9492	9.9493
	Exact	4.4430	7.0250	7.0250	8.8860	9.9350	9.9350
[37]							

**Table 4 The dimensionless frequency coefficient  $\nu$  of a SSSS plate ( $h/a=0.1$ )**

Mesh	Method	Mode number					
		1	2	3	4	5	6
4×4	FEM	4.7556	7.4493	8.1649	9.6534	10.9393	11.3686
	CS-FEM	4.4032	6.7790	6.8435	8.3901	9.0714	9.0889
8×8	FEM	4.4526	6.9470	7.0927	8.8583	9.8241	9.9006
	CS-FEM	4.3743	6.7560	6.7712	8.3830	9.2329	9.2341
16×16	FEM	4.3861	6.7950	6.8252	8.4862	9.3746	9.3788
	CS-FEM	4.3683	6.7470	6.7511	8.3623	9.2256	9.2257
20×20	FEM	4.3788	6.7766	6.7954	8.4386	9.3195	9.3211
	CS-FEM	4.3676	6.7460	6.7486	8.3595	9.2242	9.2243
	Exact	4.37	6.74	6.74	8.35	9.22	9.22
[37]							

**Table 5 The dimensionless frequency coefficient  $\nu$  of a CCC plate ( $h/a=0.005$ )**

Mesh	Method	Mode number					
		1	2	3	4	5	6
4×4	FEM	6.8025	9.5749	10.4873	11.7647	13.1176	13.5040
	CS-FEM	6.1712	8.6783	8.9731	10.3804	11.0673	11.2107
8×8	FEM	6.2735	9.0386	9.3955	11.5044	12.7057	12.9603
	CS-FEM	6.0475	8.6471	8.7198	10.5863	11.7010	11.7459
16×16	FEM	6.0709	8.6976	8.7894	10.7738	11.8234	11.8616
	CS-FEM	6.0101	8.5862	8.6030	10.4502	11.5285	11.5556
20×20	FEM	6.0446	8.6504	8.7090	10.6462	11.6973	11.7265

CS-FEM	6.0057	8.5784	8.5891	10.4317	11.5059	11.5328
Exact	5.999	8.568	8.568	10.407	11.472	11.498
[37]						

**Table 6 The dimensionless frequency coefficient  $\nu$  of a CCCC plate ( $h/a=0.1$ )**

Mesh	Method	Mode number					
		1	2	3	4	5	6
4×4	FEM	6.2704	8.5690	9.2591	10.3480	11.3969	11.7235
	CS-FEM	5.8163	7.8647	8.0481	9.2126	9.6233	9.7156
8×8	FEM	5.8578	8.1344	8.3480	9.8978	10.7828	10.9282
	CS-FEM	5.7350	7.9027	7.9501	9.3817	10.1442	10.2003
16×16	FEM	5.7402	7.9437	7.9937	9.4901	10.3007	10.3528
	CS-FEM	5.7117	7.8846	7.8965	9.3442	10.1319	10.1803
20×20	FEM	5.7267	7.9197	7.9513	9.4319	10.2369	10.2858
	CS-FEM	5.7087	7.8819	7.8895	9.3378	10.1284	10.1766
	Exact	5.71	7.88	7.88	9.33	10.13	10.18
[37]							

**Table 7 The dimensionless frequency coefficient  $\nu$  of a thin plate (aspect ratio  $h/a=0.005$ ) with various boundary conditions**

Boundary type	Mode number			
	1	2	3	4
SSSF	3.4168	5.2565	6.4200	7.6802
Exact[37]	3.4176	5.2684	6.4185	7.6854
SFSF	3.1033	4.0072	6.0235	6.2430
Exact[37]	3.1034	4.0168	6.0602	6.2406
CCCF	4.8945	6.3176	7.9672	8.7349
Exact[37]	4.9010	6.3276	7.9682	8.7613
CFCF	4.7131	5.1372	6.5755	7.8384
Exact[37]	4.7193	5.1506	6.6079	8.0291
CFSF	3.8994	4.5307	6.2707	7.0404
Exact[37]	3.9096	4.5468	6.3152	7.0356

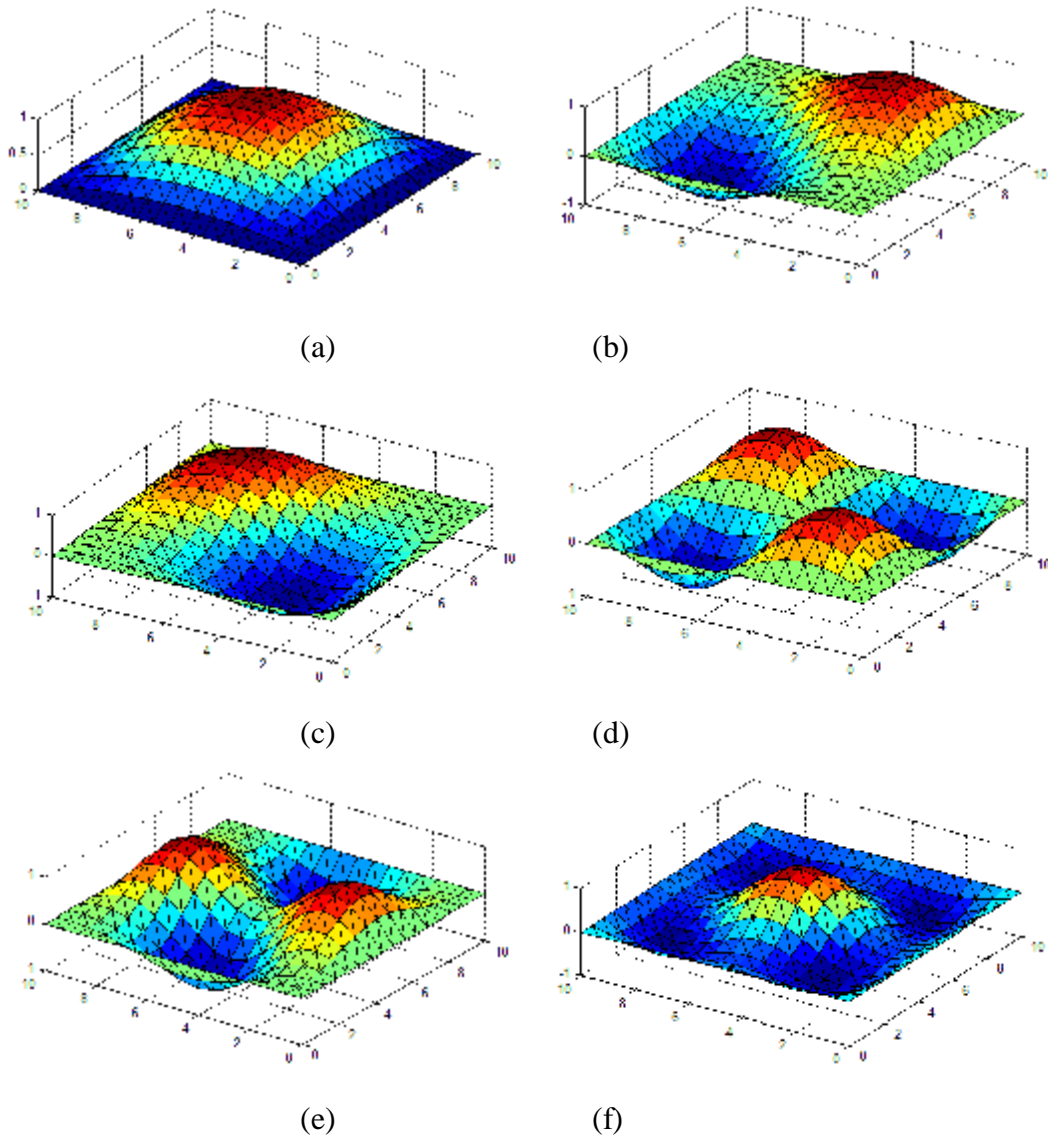


**Fig. 7 The six lowest shape modes of thin plate (aspect ratio  $h/a=0.005$ ) with SSSS boundary condition. (a)-(h): 1-8 shape modes**

### 5.3 Free vibration analysis of a rotating cantilever Mindlin plate

In order to examine the efficiency of the CS-FEM, the results are compared with those of FEM and AMM which are based on Kirchhoff plate theory. The plate is discretized with  $2 \times 16 \times 16$  triangular elements in CS-FEM and FEM. Five cantilever beam mode functions and seven free-free beam mode functions are combined to generate 35 plate mode functions in AMM according to reference [11]. Table 8 shows the lowest five dimensionless natural frequencies with  $d=1, h=0.01$  and  $s=0$ . It is seen that the dimensionless natural frequencies increase with the increasing angular velocity. Under the same angular velocity, the results of AMM is bigger than those of FEM, which means AMM provides stiffer results if using the same modeling theory. The results of CS-FEM are always smaller than the other two methods. That means the Mindlin plate theory make the structure become softer because of considering the shear deformation. In other words, the Kirchhoff plate theory is always overvalued on the

natural frequencies of the structure. Table 9 shows the lowest five dimensionless natural frequencies with  $d=1$ ,  $h=0.01$  and  $s=1$ . The same comments obtained above can be confirmed again. Compared with the results in Table 8, it is observed that the dimensionless natural frequencies increase with the increasing hub radius.

**Table 8 Five lowest dimensionless natural frequencies of a rotating plate**  
( $d=1, h=0.01, s=0$ )

Non-dimensional angular velocity	Mode	CS-FEM	FEM	AMM
$g = 1$	1	3.4963	3.4983	3.5156
	2	8.4799	8.5215	8.5328
	3	21.3255	21.4703	21.520
	4	27.0454	27.1473	27.353
	5	30.8780	31.0911	31.206
$g = 2$	1	3.5751	3.5760	3.5963
	2	8.4901	8.5357	8.5507
	3	21.6413	21.8101	21.865
	4	27.0245	27.1756	27.384
	5	31.1047	31.3537	31.477

**Table 9 Five lowest dimensionless natural frequencies of a rotating plate**  
( $d=1, h=0.01, s=1$ )

Non-dimensional angular velocity	Mode	CS-FEM	FEM	AMM
$g = 1$	1	3.7127	3.7151	3.7324
	2	8.5944	8.6112	8.6240
	3	21.4835	21.6533	21.706
	4	27.0333	27.183	27.394
	5	30.9789	31.2315	31.350
$g = 2$	1	4.3615	4.3670	4.3805
	2	8.8492	8.8878	8.9087
	3	22.3442	22.5107	22.580
	4	27.2023	27.3434	27.557
	5	31.6681	31.9054	32.043

Fig.8 shows the five lowest dimensionless natural frequencies of a rotating cantilever plate( $d = 5$ ,  $h = 0.01$ ,  $s = 1$ ) using CS-FEM versus angular velocity. It is seen that the

second and third frequency loci approach each other as the angular velocity increases and then veer away from each other. This interesting phenomenon is referred to as eigenvalue loci veering and was first discussed by Leissa [38]. Yoo [11] said these two frequency loci crossed each other between symmetric and skew-symmetric modes. However, it can be found from Fig.8(b) that they are only very closely each other and the eigenvalue crossing doesn't occur. Compared with reference [11] using AMM, the results of CS-FEM are milder.

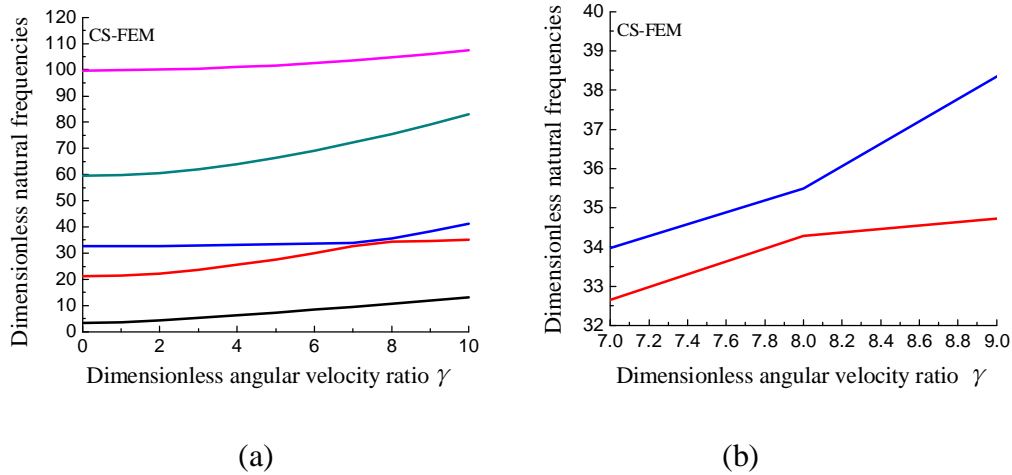
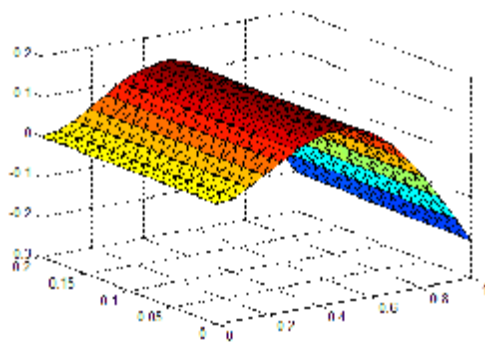
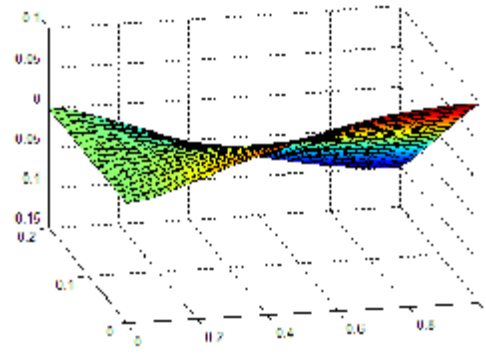


**Fig. 8 The five lowest dimensionless natural frequencies of a rotating cantilever plate versus angular velocity ( $d = 5$ ,  $h = 0.01$ ,  $s = 1$ )**

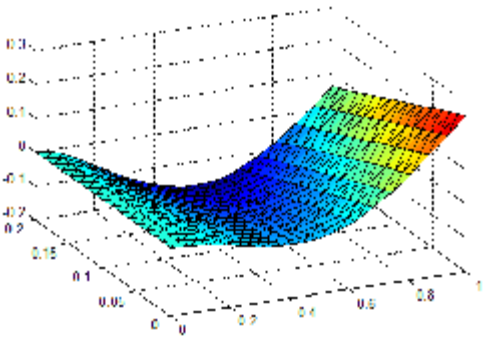
Fig.9 shows the second and third vibration modes in the veering region when the non-dimensional angular velocity is 7, 7.58, 7.6 and 8 with  $d = 5$ ,  $h = 0.01$  and  $s = 1$ , respectively. When the non-dimensional angular velocity is 7, it is clearly observed from figs.(a) and (b) that the second mode is bending mode and the third mode is torsion mode. When the non-dimensional angular velocity is 8, it is clearly observed from figs. (g) and (h) that the second mode is torsion mode and the third mode is bending mode. This phenomenon means that the second and third modes switch their shapes when the non-dimensional angular velocity changes from 7 to 8. This switching phenomenon does not occur suddenly but has a process. It is clearly seen from figs.(c),(d),(e) and (f) that there are both bending and torsion modes in the second and third modes. When the non-dimensional angular velocity is 7.58, the bending effect is greater than the torsion effect for the second mode and the torsion effect is greater than the bending effect for the third mode. That means the torsion effect is increasing for the second mode and the bending effect is increasing for the third mode when the non-dimensional angular velocity increases in the veering region. When the non-dimensional angular velocity is 7.6, we see the opposite situation, which the torsion effect is greater than the bending effect for the second mode and the bending effect is greater than the torsion effect for the third mode. Finally, when the non-dimensional angular velocity increases to 8, the switching process is complete.



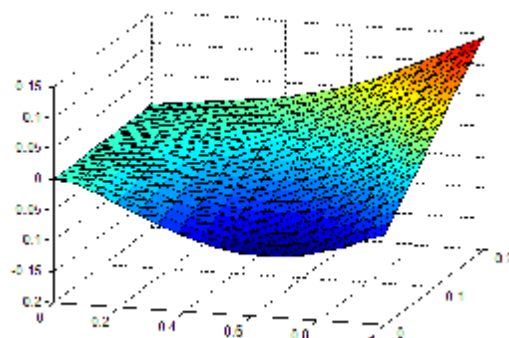
(a)  $g=7$  Second mode



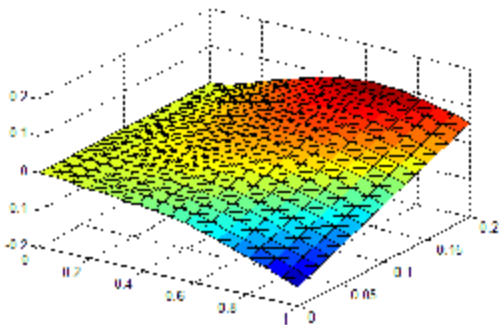
(b)  $g=7$  Third mode



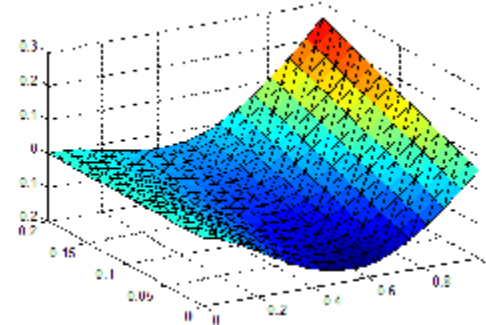
(c)  $g=7.58$  Second mode



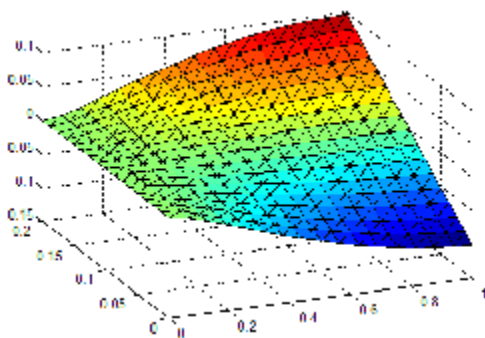
(d)  $g=7.58$  Third mode



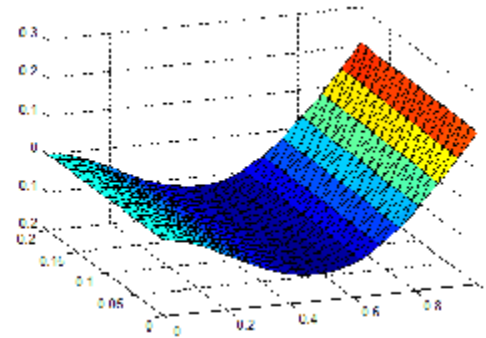
(e)  $g=7.6$  Second mode



(f)  $g=7.6$  Third mode



(g)  $g=8$  Second mode

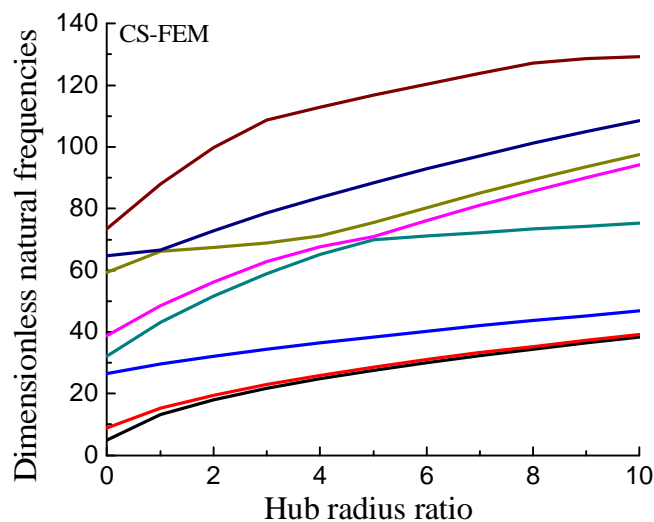


(h)  $g=8$  Third mode

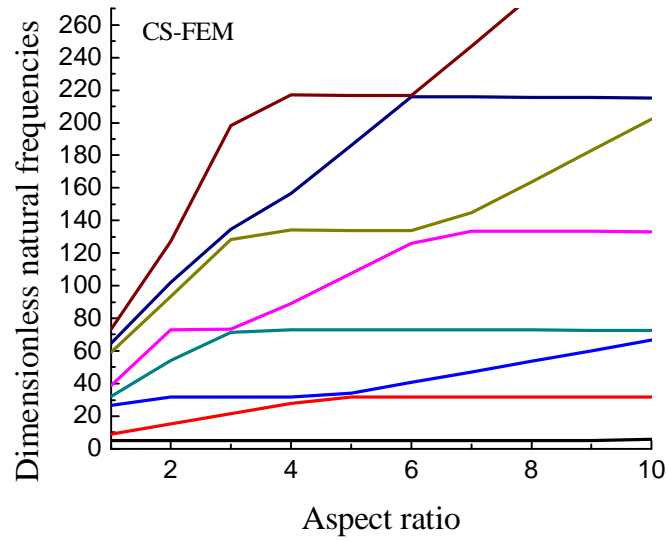
**Fig. 9 The second and third vibration modes of a rotating cantilever plate**  
 $(d = 5, h = 0.01, s = 1)$

Fig.10 shows the eight lowest dimensionless natural frequencies of a rotating cantilever

plate( $d = 1$ ,  $h = 0.01$ ,  $g = 10$ ) versus hub radius ratio  $s$ . It is seen that the dimensionless natural frequencies increase as the hub radius ratio increases. The first two frequencies are very closely. The frequency loci veering occurs from the fourth to seventh natural frequencies and there are two veering phenomena in the sixth natural frequency. Fig.11 shows the eight lowest dimensionless natural frequencies of a rotating cantilever plate( $s = 0$ ,  $h = 0.01$ ,  $g = 10$ ) versus aspect ratio  $d$ . It is observed that there are many abrupt frequency loci veering phenomena. Compared with fig.10, the aspect ratio has a greater effect on the frequency loci veering phenomena than the hub radius ratio. Fig.12 shows the eight lowest dimensionless natural frequencies of a rotating cantilever plate ( $d = 1$ ,  $s = 0$ ,  $g = 10$ ) versus thickness ratio  $h$ . The results of FEM are based on Kirchhoff plate theory and those of CS-FEM are based on Mindlin plate theory. It is seen that the results of FEM are constant and they don't change with the thickness ratio. However, the results of CS-FEM decrease as the thickness ratio increases. In the low order frequencies, the results of these two modeling theories are very closely, which means different modeling theories have a small effect on low order frequencies but have a great effect on high order frequencies. In addition, the results of CS-FEM are always smaller than those of FEM and this is confirmed again that the Kirchhoff theory overestimates the structural dynamic characteristics.



**Fig. 10 The eight lowest dimensionless natural frequencies of a rotating cantilever plate versus hub radius ratio  $s$  ( $d = 1$ ,  $h = 0.01$ ,  $g = 10$ )**



**Fig. 11** The eight lowest dimensionless natural frequencies of a rotating cantilever plate versus aspect ratio  $d$  ( $s = 0, h = 0.01, g = 10$ )

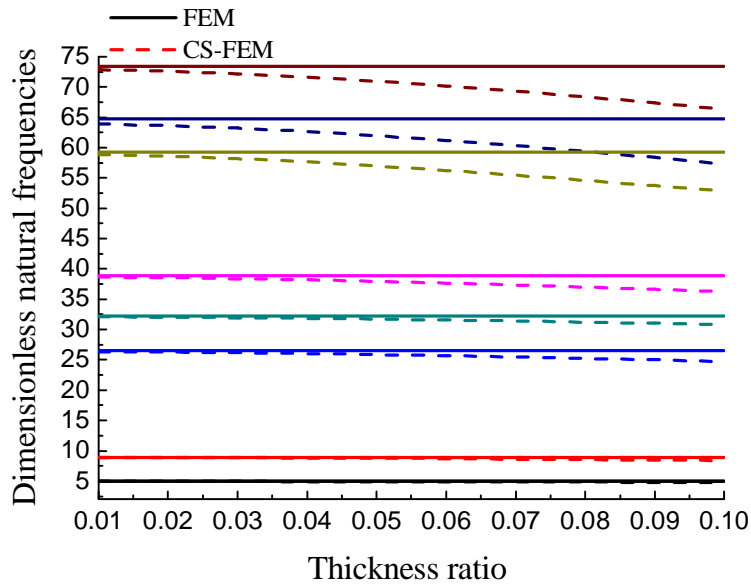


**Fig. 12** The eight lowest dimensionless natural frequencies of a rotating cantilever plate versus thickness ratio  $h$  ( $d = 1, s = 0, g = 10$ )

## 6 Conclusion

In this paper, a cell-based smoothed finite element method (CS-FEM) is formulated for non-linear free vibration analysis of rotating Mindlin plates. In order to overcome the shear locking problem, the discrete shear gap (DSG) method is used. The static cases and free vibration analysis of plates with various boundary conditions demonstrate the effectiveness of the CS-FEM. It is found that the CS-FEM based on Mindlin plate theory can provide more

accurate and “softer” solution compared with those of the conventional FEM even if using coarse meshes. For the analysis of free vibration of a rotating cantilever plate, the CS-FEM results are compared with the FEM and AMM. It is found that the natural frequencies of neighboring modes may “kissing” each other, when the angular velocity, aspect ratio and hub radius ratio changes, but they do not go cross. At the frequency kissing point, the vibration modes switch. It is also found that because of the use of the Mindlin plate theory, the natural frequencies decrease as the thickness ratio increases, which is not observed when the Kirchhoff plate theory is used. Moreover, the effect of thickness ratio is more significant in high order frequencies.

### **Acknowledgment**

The authors are grateful for the support from the National Natural Science Foundation of China (Grant Nos. 11272155, 11132007, 11502113), the 333 Project of Jiangsu Province, China (Grant No. BRA2011172), the Fundamental Research Funds for the Central Universities of China (Grant No. 30920130112009), the innovation of postgraduate education project of Jiangsu Province, China (Grant No. KYLX15\_0404), and the China Scholarship Council for one year study at the University of Cincinnati.

### **References**

- [1] R. Southwell and F. Gough, The free transverse vibration of airscrew blades, *British A.R.C. Reports and Memoranda* No. 766 (1921).
- [2] H.H. Yoo, R.R. Ryan, R.A. Scott, Dynamics of flexible beams undergoing overall motions, *Journal of Sound and Vibration* 181 (1995) 261-278.
- [3] H.H. Yoo, S.H. Shin, Vibration analysis of rotating cantilever beams, *Journal of Sound and Vibration* 212 (1998) 807-828.
- [4] L. Li, D.G. Zhang, W.D. Zhu, Free vibration analysis of a rotating hub-functionally graded material beam system with the dynamic stiffening effect, *Journal of Sound and Vibration* 333 (2014) 1526-1541.
- [5] J. Chung, H.H. Yoo, Dynamic analysis of a rotating cantilever beam by using the finite element method, *Journal of Sound and Vibration* 249 (2002) 147-164.
- [6] H. Du, M.K. Lira, K.M. Liew, A nonlinear finite element model for dynamics of flexible manipulators, *Mech. Mach. Theory* 31 (1996) 1109-1119.
- [7] G.G. Sanborn, A.A. Shabana, A rational finite element method based on the absolute nodal coordinate formulation, *Nonlinear Dynamics* 58 (2009) 565-572.
- [8] M.A. Dokainish, S. Rawtani, Vibration analysis of rotating cantilever plates, *International Journal for Numerical Methods in Engineering* 3 (1971) 233-248.
- [9] V. Ramamurti, R. Kielb, Natural frequencies of twisted rotating plates, *Journal of Sound and Vibration* 97 (1984) 429-449.
- [10] H.H. Yoo, J. Chung, Dynamics of rectangular plate undergoing prescribed overall motions, *Journal of Sound and Vibration* 280 (2005) 531-553.
- [11] H.H. Yoo, C. Pierre, Modal characteristic of a rotating rectangular cantilever plate, *Journal of Sound and Vibration* 259 (2003) 81-96.
- [12] S.H. Hashemi, S. Farhadi, S. Carra, Free vibration analysis of rotating thick plates, *Journal of Sound and Vibration* 323 (2009) 366-384.
- [13] G.R. Liu, T. Nguyen-Thoi, Smoothed finite element methods, CRC Press: Taylor and Francis Group, New York, 2010.

- [14] G.R. Liu, K.Y. Dai, T. Nguyen-Thoi, A smoothed finite element for mechanics problems, *Computational Mechanics* 39 (2007) 859-877.
- [15] K.Y. Dai, G.R. Liu, Free and forced vibration analysis using the smoothed finite element method (SFEM), *Journal of Sound and Vibration* 301 (2007) 803-820.
- [16] G.R. Liu, T. Nguyen-Thoi, K.Y. Dai, *et al*, Theoretical aspects of the smoothed finite element method (SFEM), *International Journal for Numerical Methods in Engineering* 71 (2007) 902-930.
- [17] G.R. Liu, T. Nguyen-Thoi, H. Nguyen-xuan, *et al*, A node-based smoothed finite element method (NS-FEM) for upper bound solutions to solid mechanics problems, *Computers and Structures* 87 (2009) 14-26.
- [18] T. Nguyen-Thoi, G.R. Liu, H. Nguyen-xuan, *et al*, Adaptive analysis using the node-based smoothed finite element method (NS-FEM), *Communications in Numerical Methods in Engineering* 27 (2009) 198-218.
- [19] T. Nguyen-Thoi, G.R. Liu, H. Nguyen-xuan, Additional properties of the node-based smoothed finite element method (NS-FEM) for solid mechanics problems, *International Journal of Computational Methods* 6 (2009) 633-666.
- [20] G.R. Liu, T. Nguyen-Thoi, K.Y. Lam, An edge-based smoothed finite element method (ES-FEM) for static, free and forced vibration analyses of solids, *Journal of Sound and Vibration* 320 (2009) 1100-1130.
- [21] T. Nguyen-Thoi, G.R. Liu, H.C. Vu-Do, *et al*, An edge-based smoothed finite element method (ES-FEM) for visco-elastoplastic analyses of 2D solids using triangular mesh, *Computational Mechanics* 45 (2009) 23-44.
- [22] T.N. Tran, G.R. Liu, T. Nguyen-Thoi, *et al*, An edge-based smoothed finite element method for primal-dual shakedown analysis of structures, *International Journal for Numerical Methods in Engineering* 82 (2010) 917-938.
- [23] T. Nguyen-Thoi, G.R. Liu, K.Y. Lam, *et al*, A face-based smoothed finite element method (FS-FEM) for 3D linear and nonlinear solid mechanics problems using 4-node tetrahedral elements, *International Journal for Numerical Methods in Engineering* 78 (2009) 324-353.
- [24] T. Nguyen-Thoi, G.R. Liu, H.C. Vu-Do, *et al*, A face-based smoothed finite element method (FS-FEM) for visco-elastoplastic analyses of 3D solids using triangular mesh, *Communications in Numerical Methods in Engineering* 198 (2009) 3479-3498.
- [25] R.H. Macneal, Derivation of element stiffness matrices by assumed strain distributions, *Nuclear Engineering and Design* 7 (1982) 3-12.
- [26] K.C. Park, G.M. Stanley, A curved C0 shell element based on assumed natural-coordinate strains, *Journal of Applied Mechanics* 53 (1986) 278-290.
- [27] F. Brezzi, K.J. Bathe, M. Fortin, Mixed-interpolated elements for Reissner-Mindlin plates, *International Journal for Numerical Methods in Engineering* 28 (1989) 1787-1801.
- [28] K.J. Bathe, E.N. Dvorkin, A four-node plate bending element based on Mindlin-Reissner plate theory and a mixed interpolation, *International Journal for Numerical Methods in Engineering* 21 (1985) 367-383.
- [29] E. Onate, O.C. Zienkiewicz, B. Suarez, R.L. Taylor, A general methodology for deriving shear constrained Reissner-Mindlin plate elements. *International Journal for Numerical Methods in Engineering* 33 (1992) 345-367.
- [30] Zengjie C, Wanji C, Refined triangular discrete Mindlin flat shell elements, *Computational Mechanics* 33 (2003) 52-60.
- [31] K.U. Bletzinger, M. Bischoff, E. Ramm, A unified approach for shear-locking free triangular and rectangular shell finite element, *Computational Mechanics* 75 (2000) 321-334.
- [32] M. Bischoff, K.U. Bletzinger, Stabilized DSG plate and shell elements, *Trends in computational structural mechanics*. CIMNE: Barcelona, Spain, 2001.
- [33] M. Lyly, R. Stenberg, T. Vihinen, A stable bilinear element for the Reissner-Mindlin plate model, *Computer*

*Methods Applied Mechanics Engineering* 110 (1993) 343-357.

- [34] A.K. Banerjee, T.R. Kane, Dynamics of a plate in large overall motion, *Journal of Applied Mechanics* 56 (1989) 887-892.
- [35] R.L. Taylor, F. Auricchio, Linked interpolation for Reissner-Mindlin plate element. Part II -a simple triangle, *International Journal for Numerical Methods in Engineering* 36 (1993) 3057-3066.
- [36] T. Nguyen-Thoi, P. Phung-Van, H. Nguyen-Xuan *et al*, A cell-based smoothed discrete shear gap method using triangular elements for static and free vibration analyses of Reissner-Mindlin plates, *International Journal for Numerical Methods in Engineering* 91 (2012) 705-741.
- [37] F. Abbassian, D.J. Dawswell, N.C. Knowles, Free vibration benchmarks, Atkins Engineering Science: Glasgow, 1987.
- [38] A. Leissa, On a curve veering aberration, *Journal of Applied Mathematics and Physics* 25 (1974) 99-111.